DOI 10.24425/aee.2025.153914

Reliability prediction analysis of catenary after icing based on Kriging model

JINGJING TIAN[1], LIGUO HU[1]✉, YING WANG[1], FENG ZHAO[1], XIAOQIANG CHEN[1], LEIJIAO GE[1,2], AIPING MA[3]

[1] *School of Automation and Electrical Engineering, Lanzhou Jiaotong University No.88, Anning West Road, Lanzhou, People's Republic of China*

[2] *School of Electrical Automation and Information Engineering, Tianjin University*

[3] *China Railway Lanzhou Group Co., Ltd.*

e-mail: ✉ *1689656335@qq.com*

(Received: 10.01.2025, revised: 14.08.2025)

Abstract: In order to ensure the safety of the train, the reliability of the catenary system in icy weather must be analyzed. The Kriging model was used to predict and analyze the reliability changes of the catenary system under three different icing conditions: rime, mixed, rime and rime. The change in icing thickness of the contact line of a high-speed railway was selected as a representative of the icing change of the catenary, and the actual icing cross-section was converted into an ice-covered cross-section under the ideal state that was easy to calculate, and the relationship between icing quality and thickness was discussed. The catenary components that are more affected by ice and snow weather are selected, the reliability of the catenary system is quantified, and the fault tree is used to analyze and construct the relevant model parameters. Compared with other catenary system reliability analysis methods, the prediction function of the Kriging model can meet the requirements of the analysis and study of catenary reliability. Comparing the simulation results of the models under the three icing conditions, it is found that the change rate of catenary reliability in the hoarfrost, mixed rime and glaze ice states increases sequentially, and the catenary reliability changes the least and causes the least harm in the hoarfrost state. The catenary reliability changes the most in the glace ice state, and the harm caused is also the most serious. The research results can further provide a reference for the selection of catenary maintenance and de-icing methods in icy weather.

Key words: catenary system, fault tree, icing, Kriging model, reliability

1. Introduction

High-speed railways are developing rapidly due to their advantages of high speed, low energy consumption, high safety, and comfortable rides [1]. Currently, the total length of China's high-speed railway network has exceeded 42 000 kilometers, with 3 200 kilometers operating at a normalized speed of 350 kilometers per hour [2]. However, the "eight vertical and eight horizontal" high-speed railway network in China is widely fragmented. The use of integrated night skylight maintenance, combined with temperature fluctuations around 0°C and high humidity, makes the contact conductor susceptible to ice formation [3]. In recent years, various changes in the natural environment have led to the frequent occurrence of ice-covered contact networks, resulting in train delays, stranded passengers, and significant economic losses. According to statistics from the China Meteorological Administration in 2023, southern regions such as Hubei, Hunan, and Guizhou have experienced a notable increase in freezing rain during winter, making the phenomenon of ice-covered contact networks particularly prominent. For instance, in Guizhou Province, the average annual number of days with ice cover can reach 15 to 20 days, with freezing rain accounting for approximately 40% of these occurrences. The duration of a single ice cover event can last up to 48 hours or more. In Hubei Province, the mountainous areas of the Exi region experience an average annual ice cover duration of about 200 hours, with ice thickness often exceeding 10 mm. In contrast, northern regions such as Heilongjiang and Jilin primarily experience hoarfrost, resulting in an average of 10 to 15 days of ice cover annually. However, due to the lower density of ice cover in these areas, the associated damage is relatively minor.

Contact network failures caused by ice cover demonstrate a significant upward trend. According to the China Railway Lanzhou Bureau Group Company Limited, from 2020 to 2023, the number of repairs related to the contact network ice overlay in the northwestern region is expected to increase by an average of 12 percent per annum. Additionally, the cost of these repairs is projected to rise from Euro 30.18 million to Euro 49.87 million. This increase is closely linked to the growing frequency of extreme weather events and the expansion of high-speed railway lines into regions characterized by low temperatures and high humidity.

The contact network is a vital component of high-speed electrified railway systems [4]. In high-speed railways, the contact network serves as the power supply line that delivers electricity from the main line to the train [5]. High-speed trains typically utilize electric traction, with pantographs drawing power from the contact network [6]. As the sole direct power source for electric locomotives, the operational reliability of the contact network is essential for ensuring the safe, reliable, and efficient operation of electrified railways [7]. However, the contact network is entirely exposed to outdoor conditions and lacks backup equipment [8]. Therefore, it is crucial to monitor the actual status of the contact network in order to enhance its operational reliability [9]. Research on the reliability changes of the contact network following ice accumulation in high-speed railways has also become increasingly important.

The primary methods employed in research on contact network reliability include Dynamic Bayesian Networks (DBN), Monte Carlo Simulation (MCS), Fault Tree Analysis (FTA), and Markov Analysis. Jiao Zhixiu *et al*. applied DBN theory to the reliability modeling and analysis of contact network systems, effectively capturing the dynamic characteristics and maintainability of these systems [10]. However, their study did not address the impact of extreme weather on the reliability of contact network systems. Chen Ziwen *et al*. focused on the contact network as

their research subject and demonstrated that MCS is well-suited for analyzing the reliability of contact network systems in high-wind areas [11]. Nonetheless, their analysis did not adequately consider the reliability of contact network systems under ice-covered conditions. Liu Runkai *et al*. proposed an evaluation model based on the Analytic Hierarchy Process (AHP) combined with the entropy weight method. This model exhibits high validity, comprehensive functionality, and is more effective in distinguishing the credibility states of contact networks [12].

The impact of contact network ice cover on the operation of high-speed railways can be categorized based on the thickness of the ice cover into four levels: general, more serious, serious, and especially serious. General ice cover primarily affects the flow quality of high-speed trains. However, when the ice cover exceeds the general level, it not only compromises the flow quality of the trains but also significantly impacts the structural reliability of the contact network.

In terms of ice cover thickness prediction calculation, Huang Xinbo *et al*. applied the fuzzy system modelling method to establish the ice cover growth prediction formula, and the maximum error between the actual ice cover thickness value and the predicted value of ice cover thickness obtained through the fuzzy system ice cover thickness prediction formula is less than 5 mm [13]. Due to the large error, the accuracy of the reliability prediction of the contact network under the relevant ice cover thickness will be reduced. Li Xianchu *et al*. proposed a kind of artificial intelligence ice cover thickness prediction model based on an adaptive mutation particle swarm optimization (AMPSO) algorithm in an optimization BP neural network, which has good engineering applicability [14], but the weather conditions and other factors rely on the larger, complex data collection, and the data collection is complicated. Weather conditions and other factors render the collected data complex, making it non-applicable for calculating the ice cover thickness of contact networks. At present, the microwave-based online ice cover monitoring system is more commonly used in the observation of contact network ice cover thickness, which has the advantages of high accuracy and sensitivity. Wu Lei *et al*. developed a straightforward chain suspension contact network finite element model using ANSYS finite element analysis software. They employed the negative chi method to analyze the static initial configuration of the contact network model, which served as the foundation for establishing the contact network ice-covering model [15]. However, they did not conduct an analysis of the reliability changes in the contact network following ice coverage. Li Junbo *et al*. focused solely on reviewing the analysis and preventive measures related to railway contact network ice overlay [16], but they did not propose an effective method for analyzing and studying the contact network ice overlay. Ling Fei *et al*. introduced a contact network ice-covering prediction method based on the Radial Basis Function (RBF) neural network. This method incorporates real-time data on air temperature, humidity, wind speed, wind direction, air pressure, and other factors to predict contact network ice coverage. In practice, this approach demonstrates faster training speed and improved robustness, generalization ability, and accuracy. However, it requires consideration of numerous factors, complicating its application in contact network analysis [17]. Wang Zhen *et al*. proposed a reliability assessment method for high-speed railway contact network systems that accounts for the influence of weather conditions. This method establishes failure rate and repair rate correction models for various components of the contact network system under three different weather states, following IEEE standard guidelines. It derives the failure and repair rates of components under varying weather conditions [18]. Nevertheless, the reliability assessment of the contact network under ice-covered conditions was not addressed.

Fritjof Nilsson *et al*. analyzed the damage to contact wires caused by ice accumulation, a common contributor to train delays in Northern Europe during the winter months. They also investigated how resistive heating can be employed to prevent ice formation on uninsulated metallic cables during this season [19]. Skrzyniarz Marek *et al*. presented a model for calculating current fluctuations and resistance values of the elements involved in the contact network under ice-covered conditions [20]. Lotfi Arefeh *et al*. investigated the impacts of ice cover on contact network systems and summarized the existing solutions to these challenges. They explored the most effective de-icing methods to minimize the effects of icing on railway operations and safety [21]. References [19–21] focus on the impact of ice overlay on the contact network system and the de-icing methods employed. However, they do not adequately explain how the reliability of the contact network system is affected by ice overlay.

Since the contact network structure becomes more complex after icing, this paper employs the Kriging model for the structural reliability prediction analysis of the contact network post-icing. The Kriging model is characterized by a small and unbiased estimation variance, making it suitable for highly nonlinear, high-dimensional complex structural systems. It has garnered significant attention in the field of reliability [22]. The thickness and weight of ice cover generated by the contact network under various weather conditions, including hoarfrost, mixed rime, and glaze ice, are utilized as variables to predict and analyze changes in the reliability of the contact network.

2. Introduction to the Kriging model

The Kriging model is an accurate and stochastic interpolation method that not only provides predicted values for unsampled points but also estimates the prediction variance. As a result, this method has been widely used in structural reliability analysis [23].

The Kriging model consists of two components: the stochastic part and the polynomial regression [24]. Its mathematical expression is as follows

$$G(\boldsymbol{X}) = f^T(\boldsymbol{X})\beta + z(\boldsymbol{X}). \tag{1}$$

In the context of the Kriging model, let $\hat{G}(\boldsymbol{X})$ represent the predicted value, and $\boldsymbol{X}$ denote any input variable. Assuming there are m sample points, labeled as $(\boldsymbol{X}_1, \boldsymbol{X}_2, \boldsymbol{X}_3, \ldots, \boldsymbol{X}_m)$, the true value can be represented as $(G(\boldsymbol{X}_1), G(\boldsymbol{X}_2), G(\boldsymbol{X}_3), \ldots G(\boldsymbol{X}_m))$. The mean of the Gaussian process is denoted by $z(\boldsymbol{X})$, which constitutes a component of the regression function. The basis function of the Kriging model is represented by $f^T(\boldsymbol{X})$, and it serves as the regression coefficient for the basis function $f^T(\boldsymbol{X})$. Additionally, $z(\boldsymbol{X})$ denotes the Gaussian stochastic process of the Kriging model, which has a mean value of 0 and a variance of σ^2.

The covariance of the stochastic process $z(\boldsymbol{X})$ can be expressed as:

$$\mathrm{Cov}\left[z(\boldsymbol{X}_i), z(\boldsymbol{X}_j)\right] = \sigma^2 R(\boldsymbol{X}_i, \boldsymbol{X}_j, \theta), \tag{2}$$

where $R(\boldsymbol{X}_i, \boldsymbol{X}_j, \theta)$ represents the correlation function between $z(\boldsymbol{X}_i)$ and $z(\boldsymbol{X}_j)$, while θ denotes the correlation parameter of $R(\boldsymbol{X}_i, \boldsymbol{X}_j, \theta)$, which can be estimated using maximum likelihood estimation.

In this paper, the Gaussian function is chosen as the correlation function of the Kriging model. Its expression is:

$$R\left(\boldsymbol{X}_i, \boldsymbol{X}_j, \theta\right) = \exp\left(-\theta\left(\boldsymbol{X}_i - \boldsymbol{X}_j\right)^2\right), \quad 0 < \theta < 2. \tag{3}$$

Based on the relationships outlined above, the expressions for the predicted response value and its variance are as follows:

$$\mu_{\hat{G}(X)} = f^T(\boldsymbol{X})\beta + \boldsymbol{r}(\boldsymbol{X})^T\boldsymbol{R}^{-1}(\boldsymbol{G} - \boldsymbol{F}\beta), \tag{4}$$

$$\hat{\sigma}^2_{\hat{G}(X)} = \sigma^2\left[1 + \boldsymbol{u}(\boldsymbol{X})^T(\boldsymbol{F}^{\mathrm{T}}\boldsymbol{R}^{-1}\boldsymbol{F})^{-1}\boldsymbol{u}(\boldsymbol{X}) - \boldsymbol{r}(\boldsymbol{X})^{\mathrm{T}}\boldsymbol{R}^{-1}\boldsymbol{r}(\boldsymbol{X})\right], \tag{5}$$

where: $\boldsymbol{F}$ represents the regression matrix, $\boldsymbol{R}$ denotes the correlation matrix, and $\boldsymbol{u}(\boldsymbol{X})$ and $\boldsymbol{r}(\boldsymbol{X})$ are defined as follows:

$$\boldsymbol{u}(\boldsymbol{X}) = \boldsymbol{F}^{\mathrm{T}}\boldsymbol{R}^{-1}\boldsymbol{r} - \boldsymbol{f}, \tag{6}$$

$$\boldsymbol{r}(\boldsymbol{X}) = \left[R(\theta, \boldsymbol{X}_1, \boldsymbol{X}), R(\theta, \boldsymbol{X}_2, \boldsymbol{X}), \cdots, R(\theta, \boldsymbol{X}_k, \boldsymbol{X})\right]. \tag{7}$$

The value of the prediction variance $\hat{\sigma}^2$ indicates the magnitude of uncertainty in the predicted value of the Kriging model at the prediction point $\boldsymbol{X}$. It serves as a crucial basis for active learning reliability methods that utilize the Kriging model [25]. When $\hat{\sigma}^2$ for an input variable $\boldsymbol{X}$ is small, it signifies that the model's prediction uncertainty for that variable is low, resulting in high reliability of the prediction results. Conversely, when $\hat{\sigma}^2$ for an input variable $\boldsymbol{X}$ is large, it indicates that the model's prediction uncertainty for that variable is high, leading to low reliability of the prediction results.

When the data from the Kriging model exhibit a non-normal distribution, the Box–Cox transformation method and the quantile normalization method can be employed to adjust the data, bringing it closer to a normal distribution. The Box–Cox transformation optimizes the data distribution using the parameter φ, and its expression is as follows:

$$Y = \begin{cases} \dfrac{X^{\varphi} - 1}{\varphi} \varphi \neq 0 \\ \ln(X)\ \varphi = 0 \end{cases}, \tag{8}$$

where Y represents the transformed data and φ denotes the transformation parameter.

The quantile normalization method, on the other hand, maps the data to the quantiles of the standard normal distribution and is suitable for multi-source data fusion scenarios. A Shapiro–Wilk test is required after transformation to ensure data normality. If normality is still not achieved, the model parameters can be adjusted in conjunction with kernel density estimation.

When the data are non-stationary, they can be processed using spatial detrending with universal Kriging. Spatial detrending employs polynomial regression or locally weighted scatterplot smoothing to identify trend terms, which are then removed from the original data. Universal Kriging incorporates the trend term directly into the Kriging model using the following expression:

$$Z(x) = \sum_{i=1}^{p} f_i(x)\beta_i + \delta(x), \tag{9}$$

where $f_i(x)$ represents the basis function and $\delta(x)$ denotes a smooth random field.

When the data exhibit a trend, time series decomposition can be employed to separate the data into three components: trend (T_t), seasonal (S_t), and random term (T_t). Subsequently, the random term is modeled using Kriging, represented by the following expression:

$$Z_t = T_t + S_t + R_t, \tag{10}$$

where Z_t represents the observed value at time point t.

3. Analysis of the contact network system after ice cover

3.1. Experimental contact line selection

Each component of the contact network has varying requirements for ice cover. Contact wires have the highest requirements, followed by bearing cables, while hanging chords and electrical connections have the lowest [26]. In this paper, the thickness of the ice cover on the contact line is chosen as a representative measure. The mass of ice cover per unit length is calculated to analyze the impact of different ice cover thicknesses on the reliability of the contact network.

The design speed of the contact line is 300 km/h to 350 km/h. It is constructed from a high-strength copper alloy, and the specific model of the contact line examined in this paper is designated as CTMH150. This model has a standard cross-sectional area of 150 mm^2, a radius of $r = 7.2$ mm, and its cross-sectional shape is illustrated in Fig. 1.

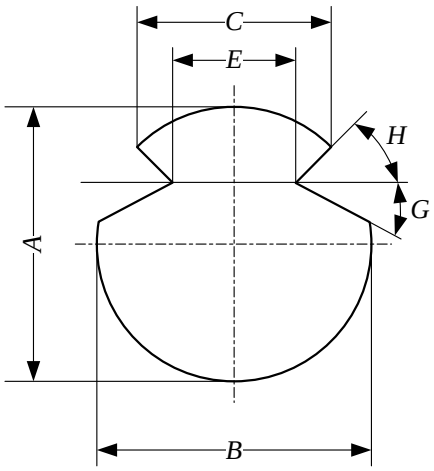

Fig. 1. CTMH150 cross-section shape: A – section diameter (height); B – section width; C – head width; E – (trench) slot tip distance; G – downward sloping angle; H – upward sloping angle

In power grid transmission lines, the hazards associated with ice accumulation primarily manifest as the collapse of power towers, insulator flashover tripping, wire breakage, and conductor-induced oscillations [27]. Once the extent of icing surpasses the anti-icing capacity of the transmission lines, the insulation performance of power equipment is significantly compromised, leading to incidents such as tripping and circuit breakage [28]. The dangers posed by icing on

contact networks are similar to those of grid icing; they not only increase the stress points and enlarge the arc of the contact network but also exacerbate the wear and tear on the pantograph sliding plate, resulting in a higher frequency of accidents such as bow scraping. Additionally, ice accumulation on the contact network can lead to insulator flashovers caused by short circuits within the network. In cases of severe icing, especially when accompanied by high winds, the contact network is at a heightened risk of oscillation, which can result in accidents such as downed poles and collapsed bows.

The types of ice that form on the railway contact network include hoarfrost, mixed rime, and glaze ice. Their densities range from 0.1 to 0.3 g/cm^3 for hoarfrost, 0.2 to 0.6 g/cm^3 for mixed rime, and 0.7 to 0.9 g/cm^3 for glaze ice [29]. Hoarfrost is characterized by dry ice growth, resulting in a small bonding point and low density, which leads to minimal harm. Mixed rime represents a transition between dry and wet growth; it has a larger bonding point, higher density, and a stronger structure, resulting in significant harm. Glaze ice, classified as wet growth, has the largest bonding point, the highest density, and the strongest structure, leading to the greatest degree of harm.

3.2. Calculation of contact line ice cover parameters

The icing process of the contact network is complex, influenced by numerous factors and requiring a multidisciplinary approach [30]. The calculation of the ice cover thickness at the contact line involves several variables, including ice cover density, shape factor, short diameter, long diameter, radius, and attachment radius. Currently, the measurement of actual ice cover thickness utilizes an online monitoring device developed based on microwave technology. This device calculates ice cover thickness by measuring the transmission time of microwave signals sent and received. The thickness is determined by comparing the time difference between the transmission time and the time required for the microwave signal to travel through air without ice cover [29]. The actual ice cover at the contact line of high-speed railway networks exhibits varying cross-sectional shapes and uneven thickness. To facilitate computational studies, it is essential to convert the actual ice cover cross-section into an idealized form with a uniform thickness and a circular cross-section, as illustrated in Fig. 2.

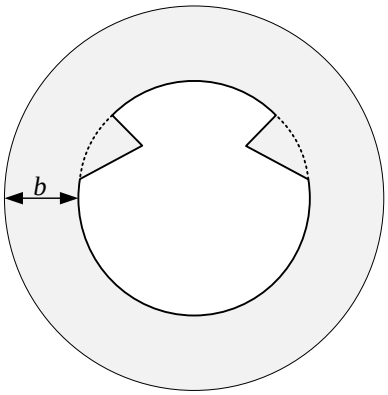

Fig. 2. Ideal icing cross-section of the contact line

According to the method for calculating the thickness of conductor ice cover described in Reference [31], the standard ice thickness is determined by examining or measuring the diameter of the ice cover, which can be expressed as follows:

$$b = \sqrt{\frac{\rho}{0.9}(K_s R^2 - r^2) + r^2} - r, \tag{11}$$

where: b represents the standard thickness of the ice cover in millimeters (mm); ρ denotes the density of ice cover, measured in grams per cubic centimeter (g/cm^3); R denotes the radius of the ice cover at the contact wire, including the attachment of the ice cover, measured in millimeters (mm); r denotes the contact wire radius in millimeters (mm); and K_S signifies the ice cover shape factor, defined as the ratio of the short diameter of the ice cover to its long diameter.

The cross-sectional area of the ice-covered portion of the contact line, i.e., the area of the shaded portion S, can be calculated from Fig. 2 as follows:

$$S = \pi(r + b)^2 - \pi r^2 + \Delta S, \tag{12}$$

where r represents the radius of the contact line CTMH150 in millimeters (mm), and ΔS denotes the area of the grooved portion of the contact line, measured in square millimeters (mm^2) with a value of $\Delta S = \pi r^2 - 150 = 12.86$.

The mass of ice cover, m(kg), per unit length l (l = 1 meter) of the contact line can be calculated using Eq. (12) with the following expression:

$$m = Sl\rho, \tag{13}$$

where ρ is the density of ice cover.

After analyzing the statistics of parameters such as ice cover density under various weather conditions [27], the details are presented in Table 1.

Table 1. Relevant parameters for different forms of icing

Type of ice cover	**Hoarfrost**	**Mixed rime**	**Glaze ice**
Densities/(g/cm^3)	0.1 ~ 0.3	0.2 ~ 0.6	0.7 ~ 0.9
Temperature/°C	–25 ~ –10	–10 ~ –2	–3 ~ 0
Air velocity/(m/s)	1 ~ 3	2 ~ 8	3 ~ 15
Radius of a droplet/(mm)	1 ~ 10	2 ~ 16	5 ~ 20
Degree of harm	Low	Moderate	High

In order to facilitate the analysis presented in this paper, we define the following ranges for ice thickness based on different weather conditions: hoarfrost with an ice thickness of 0 to 10 mm, mixed rime with an ice thickness of 5 to 15 mm, and glaze ice with an ice thickness of 10 to 25 mm. According to Table 1, the density parameters for the various forms of ice cover are established. These parameters will be incorporated into Formulas (12) and (13), resulting in the relationship between ice thickness and the quality of the ice cover, as illustrated in Fig. 3.

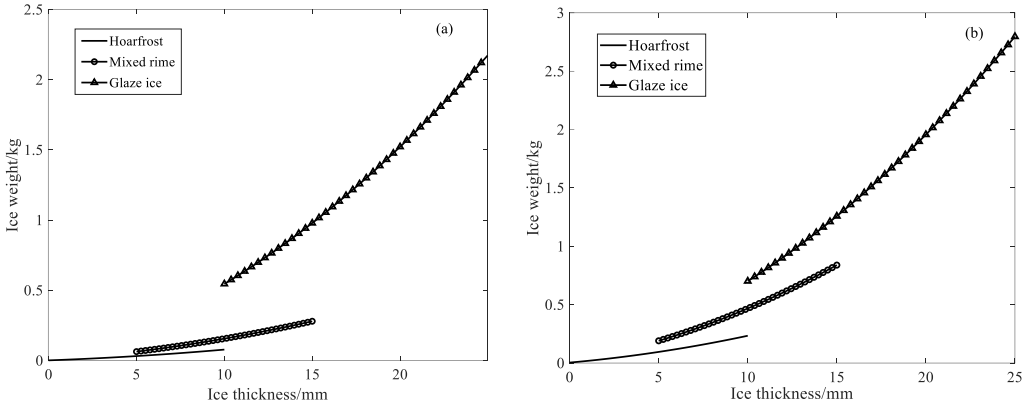

Fig. 3. Relationship curve between ice thickness and ice weight: minimum density of ice cover for each state (a); taking the highest density of ice cover for each state (b)

From Fig. 3, it is evident that as ice thickness increases, the quality of the ice cover also rises significantly. The growth rate of ice cover quality is slow during hoarfrost conditions, while the growth rate is higher in mixed rime conditions. The highest growth rate occurs during glaze ice, indicating that glaze ice poses the greatest hazard to the contact network from this perspective.

In this paper, we focus on the maximum value of ice cover density under various ice cover conditions. The subsequent data extraction stage is conducted based on the following ice cover densities: $\rho_1 = 0.3$ g/cm^3, $\rho_2 = 0.6$ g/cm^3, $\rho_3 = 0.9$ g/cm^3.

4. Quantification of reliability after contact network ice coverage

According to the fundamental structure of the contact network system, it can be viewed as a system composed of four subsystems arranged in series: the strut and foundation, the support device, the contact suspension, and the positioning device. Various components are connected in series to form the corresponding subsystems. It is assumed that the contact network system and its components can exist in two states: 'normal' and 'failure'. Since this is a series system, the failure of any single component will result in the entire contact network system losing its ability to function properly [14].

When modeling the reliability prediction of contact network icing, considering all components in the contact network significantly increases the complexity of the modeling process. Therefore, it is advisable to focus on selecting the components within each subsystem that are most affected by icing. For the time being, pillars and foundations can be excluded from consideration due to their high design standards and minimal impact on the stable operation of the contact network during snow and ice conditions. Support insulators will be chosen for the support devices, while additional conductors, contact wires, bearing cables, and suspension strings will be selected for the contact suspension system. Positioners will be designated for the positioning devices.

There is a close relationship between ice cover at contact lines and the failure rates of contact network components, with each factor exacerbating equipment losses or triggering mechanical and electrical failures through various physical mechanisms. When ice cover forms at low temperatures, the weight of the ice exerts additional mechanical loads on the conductor, leading to increased wire sag and excessive tension, which can result in wire breakage or insulator fractures. Low temperatures can also cause a decrease in the tensile strength of metals, thereby increasing the likelihood of component failures. Additionally, when humidity rises, metal surfaces can easily develop an electrolyte film, which induces galvanic corrosion and further elevates the failure rates of components. Wind speeds can cause ice-covered wires to sway, resulting in fatigue breakage of positioners, wear and tear on suspension strings, and other faults. Increased intensity of rain and snow can thicken the ice on contact wires, triggering offline discharges in the bow network and causing abnormal wear of the pantograph carbon slide plates, which leads to a higher failure rate of the contact network system. An increased current load will cause the wire to heat up; although this can inhibit ice formation, prolonged high temperatures will accelerate the creep of the lead. Consequently, the annual elongation of the contact line will increase, leading to the failure of the anchor segment joint compensation and further raising the failure rate of the contact network components.

After querying statistics and historical fault records, we obtained data on the failure rates of each component in a section of the high-speed railway contact network affected by snow and ice conditions, as shown in Table 2.

Table 2. The failure rate of each component in ice and snow weather

Serial number	**Type of component**	**Failure rate λ(‰)**
X_1	Catenary wire	2.3
X_2	Auxiliary wire	0.4
X_3	Support insulator	1.15
X_4	Dropper	0.7
X_5	Contact wire	2
X_6	Steady arm	0.5
X_7	Trip/Power outage	1.5

For quantifying the reliability of the contact network, the fault tree method can be employed for analysis, significantly simplifying the modeling process. The seven components listed in Table 2 are in an ice-covered state, which has a substantial impact on the reliability of the contact network. The effects of other components, which are less significant, can be temporarily disregarded. Consequently, the fault tree for the ice-covered contact network is established, as illustrated in Fig. 4.

Without accounting for the aging of the contact network components over time or the damage caused by the intrusion of foreign objects, the reliability of each component in the contact network is assumed to be 1. For the purpose of analysis, the component failure rate presented in Table 2 is based on statistical calculations conducted under an ice cover thickness of 5 mm. Assuming that the

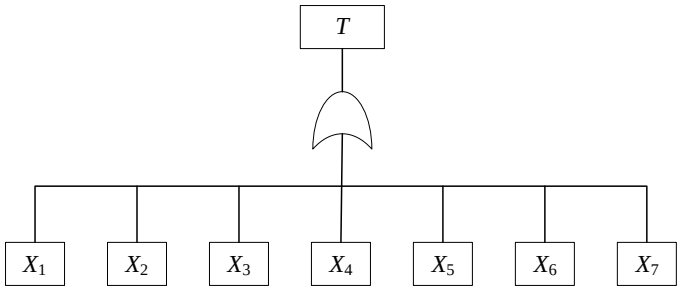

Fig. 4. Vertical acceleration of ballastless track structure with short sleeper

failure rate of various components in the contact network is linearly related to the quality of the ice cover per unit length, the reliability of each component, denoted as R_i, can be expressed as follows:

$$R_i = 1 - m\frac{\lambda_i}{m_0}, \tag{14}$$

where m_0 represents the initial ice cover mass and m denotes the actual ice cover mass.

After calculating the reliability of each component using Eq. (14), it can be observed from the fault tree in Fig. 4 that there is a series relationship among the reliabilities of the individual components. Consequently, the overall reliability R of the contact network can be determined using the following expression:

$$R = \prod_{i=1}^{7} R_i. \tag{15}$$

5. Kriging model predictive analysis

Based on the relationship between ice cover thickness and ice cover quality illustrated in Fig. 3, along with the corresponding contact network reliability derived from Eq. (15), the correlation matrix can be established as follows:

$$\begin{cases} \boldsymbol{B} = (b_1, b_2, b_3, \ldots, b_n)^T \\ \boldsymbol{M} = (m_1, m_2, m_3, \ldots, m_n)^T \\ \boldsymbol{R} = (r_1, r_2, r_3, \ldots, r_n)^T \end{cases}, \tag{16}$$

where: $\boldsymbol{B}$ represents the ice cover thickness matrix, $\boldsymbol{M}$ denotes the ice cover weight matrix, and $\boldsymbol{R}$ signifies the contact network ice cover reliability matrix.

In this study, we analyze three distinct ice cover states corresponding to the ice cover thickness, ice cover quality, and ice cover reliability data, each uniformly selected with $n = 40$ parameters as the elements of the matrices. We employed MATLAB to develop the Kriging model program, utilizing the DACE toolbox, which is a commonly used tool for this purpose. The zero-order polynomial regression and Gaussian correlation function available in DACE were applied to fit the Kriging model. The matrices $\boldsymbol{B}$, $\boldsymbol{M}$, and $\boldsymbol{R}$, obtained under conditions of hoarfrost, mixed rime, and glaze ice, were substituted into the Kriging model, and the procedure was executed. The results of the analysis are presented in Figs. 5–7.

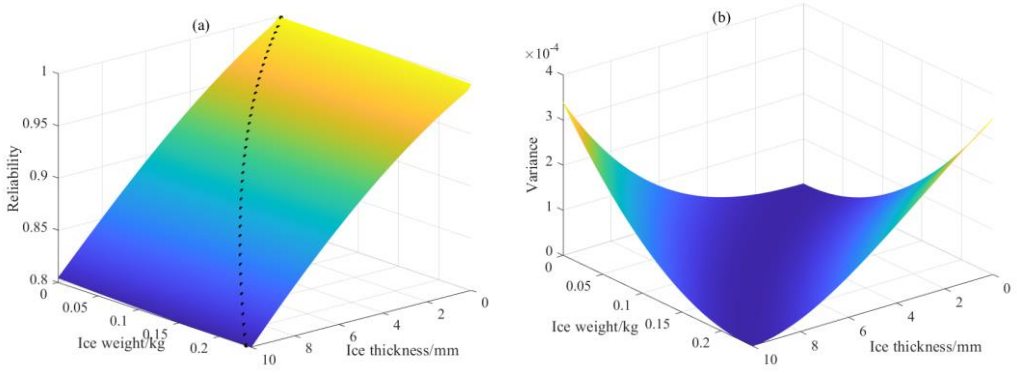

Fig. 5. Results of hoarfrost icing runs: contact network reliability changes (a); forecast variance (b)

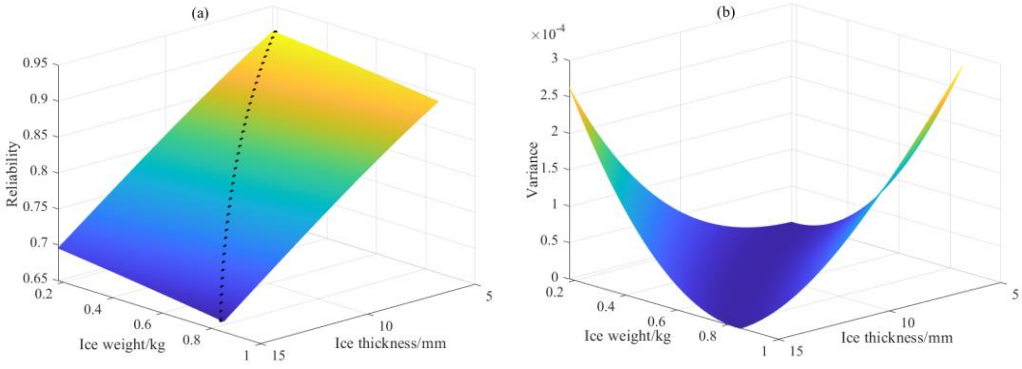

Fig. 6. Results of mixed rime icing runs: contact network reliability changes (a); forecast variance (b)

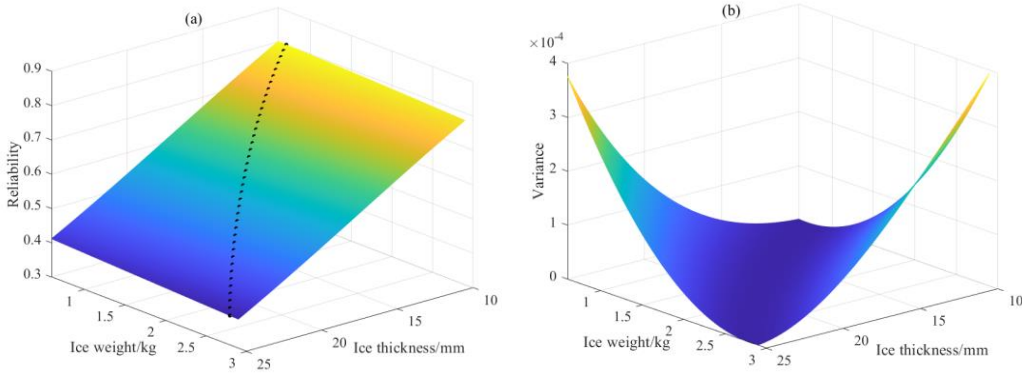

Fig. 7. Results of glaze icing runs: contact network reliability changes (a); forecast variance (b)

The shape of the surface in Fig. 5(a) illustrates the model's fit to the data. The reliability exhibits a decreasing trend as both the thickness and quality of the ice cover increase under hoarfrost conditions. When the ice cover thickness rises from 0 to 10 mm, the reliability of the contact network declines from 1 to 0.8, while the surface smoothing aligns closely with expectations, indicating a good model fit. At this point, appropriate de-icing measures can be implemented to enhance the reliability of the contact network in response to the observed changes in reliability. The area with low prediction variance, as shown in the surface of Fig. 5(b), corresponds to the region of reliable predictions in Fig. 5(a). This indicates that the prediction uncertainty of the Kriging model in this area is low, resulting in high reliability of the prediction outcomes. Conversely, the area with high prediction variance in the surface corresponds to the region of unreliable predictions in Fig. 5(c), suggesting that the prediction uncertainty of the Kriging model in this area is high, leading to low reliability of the prediction results.

The predicted value surface in Fig. 6(a) indicates that the reliability of the contact network decreases from 0.91 to 0.66 as the ice cover thickness increases from 5 mm to 15 mm under mixed rime conditions. The surface smoothing aligns closely with expectations, demonstrating a strong model fit. Additionally, the results of the analysis of the predicted variance surface in Fig. 6(b) are consistent with those presented in Fig. 6(b).

The predicted value surface in Fig. 7(a) indicates that the reliability of the contact network decreases from 0.8 to 0.38 as the thickness of the ice cover under glaze ice conditions increases from 10 mm to 25 mm. The surface smoothing aligns closely with expectations, demonstrating a strong model fit. Additionally, the analysis results of the prediction variance surface in Fig. 7(b) are consistent with those presented in Fig. 5(b).

Reliability for traction vehicle operators and contact network operators refers to the overall capability of the contact network to sustain power transmission and mechanical stability in ice-covered environments. The reliability of the contact network, as assessed by the Kriging model, can offer operators scientific support for risk warnings, operational and maintenance strategies, and de-icing methods. Ultimately, this ensures the safe and timely operation of trains.

According to the classification of contact network reliability in Reference [12], the reliability threshold value for the contact network system of high-speed railways can be established at 0.9 under ice-covered conditions. When R is in the range of 0.9 to 1, the thickness of the contact line ice cover during hoarfrost conditions varies from 0 to 5.6 mm, whereas in mixed rime conditions, it ranges from 5 to 5.5 mm. In these situations, it is recommended that high-speed trains reduce their speed. Additionally, copper-based powder carbon sliding plate pantographs should be installed on the moving train sets to scrape off the ice. The railway department should also enhance daily monitoring and testing efforts [12]. When R falls below 0.9, to ensure passenger safety, it is advised that high-speed trains cease operations, and the railway department should implement appropriate de-icing measures for the high-speed railway contact network.

6. Conclusions

Applying the Kriging model to predict the reliability of contact networks after ice overlay effectively utilizes the model's low variance and unbiased estimation capabilities. This approach is well-suited for the complex structural systems inherent in contact networks and introduces a novel method for assessing the reliability of these systems.

Based on the prediction model for the reliability of contact network icing, the predictive capability of the Kriging model is employed to analyze the trend of reliability in the contact network system concerning the thickness and quality of icing. It was observed that the change in contact network reliability during hoarfrost conditions is minimal, ultimately stabilizing at a reliability level of 0.8. This suggests that the impact of freezing weather on the reliability of the contact network system is relatively minor. In contrast, the reliability of the contact network during glaze ice experiences significant fluctuations, ultimately decreasing to 0.38. This indicates that freezing rain has a considerably more severe impact on the reliability of the contact network system.

According to the Kriging model, the prediction results for the reliability of the contact network under ice conditions can inform subsequent de-icing methods. For instance, when the monitored ice thickness is minimal, the reliability of the contact network system is not significantly affected, allowing for the use of copper-based powder for skateboard pantograph de-icing. Conversely, when the monitored ice thickness is substantial, it severely impacts the reliability of the contact network system. In such cases, artificial de-icing or thermodynamic de-icing methods should be employed.

References

[1] Li Biyu, Kang Gaoqiang, Wang Hu *et al.*, *Toward Reliable high-speed railway pantograph-catenary system state detection: Multitask deep neural networks with runtime reliability monitoring*, IEEE Transactions on Instrumentation and Measurement, vol. 73, pp. 1–11 (2024), DOI: 10.1109/TIM.2023.3334367.

[2] Zhao Liqin, *Research on the Impact and Transmission Path of China's High-Speed Rail on Regional Carbon Emissions*, [D], Shijiazhuang Tiedao University (in Chinese) (2024), DOI: 10.27334/d.cnki.gstdy.2024.000090.

[3] SHI Guoqiang, *DC ice melting technology for high-speed railway catenary*, China Railways (in Chinese), vol. 11, pp. 122–127 (2020), DOI: 10.19549/j.issn.1001-683x.2020.11.122.

[4] Cheng Hongbo, Cao Yufan, Wang Jiaxin *et al.*, *A preventive, opportunistic maintenance strategy for the catenary system of high-speed railways based on reliability*, J. Proceedings of the Institution of Mechanical Engineers, Part F: Journal of Rail and Rapid Transit, vol. 234, no. 10, pp. 1149–1155 (2020), DOI: 10.1177/0954409719884215.

[5] Zhao Hongwei, Wu Siquan, Tian Zhen *et al.*, *Context-guided coarse-to-fine detection model for bird nest detection on high-speed railway catenary*, Multimedia Systems, vol. 29, no. 5, pp. 2729–2746 (2023), DOI: 10.1007/s00530-023-01119-5.

[6] Liu Zhigang, Wang Hui, Chen Hongtian *et al.*, *Active pantograph in high-speed railway: Review, challenges, and applications*, Control Engineering Practice, vol. 141, 105692 (2023), DOI: 10.1016/j.conengprac.2023.105692.

[7] Wang Jiapei, Gao Shibin, Yan Ziwei *et al.*, *Operational reliability analysis of catenary based on Bayesian network*, Electrified Railways (in Chinese), vol. 28, no. 5, pp. 63–68+74 (2017), DOI: 10.19587/j.cnki.1007-936x.2017.05.015.

[8] Feng Ding, Yu Qinyang, Sun Xiaojun *et al.*, *Risk assessment for electrified railway catenary system under comprehensive influence of geographical and meteorological factors*, J. IEEE Transactions on Transportation Electrification, vol. 7, no. 4, pp. 3137–3148 (2021), DOI: 10.1109/TTE.2021.3078215.

[9] Yi Lingzhi, Zhao Jian, Yu Wenxin *et al.*, *Health status evaluation of catenary based on normal fuzzy matter-element and game theory*, J. Journal of Electrical Engineering & Technology, vol. 15, no. 5, pp. 2373–2385 (2020), DOI: 10.1007/s42835-020-00481-y.

[10] Jiao Xiuzhi, Yu Long, *Research on the reliability of catenary system based on dynamic Bayesian network*, Journal of Railway Science and Engineering (in Chinese), vol. 18, no. 11, pp. 3040–3047 (2021), DOI: 10.19713/j.cnki.43-1423/u.T20201146.

[11] Chen Ziwen, Wang Yanzhe, Chen Ke, *Reliability analysis of catenary system in windy area based on Monte Carlo method*, Electrified Railways (in Chinese), vol. 33, no. 5, pp. 36–39+44 (2022), DOI: 10.19587/j.cnki.1007-936x.2022.05.008.

[12] Liu Runkai, Yu Long, Chen Deming, *Research on Credibility Evaluation of High-speed Railway Catenary Based on AHP-Entropy Weight Method*, Journal of Railway Science and Engineering (in Chinese), vol. 16, no. 8, pp. 1882–1889 (2019), DOI: 10.19713/j.cnki.43-1423/u.2019.08.003.

[13] Huang Xinbo, Li Jiajie, Ouyang Lisha *et al.*, *Icing Thickness Prediction Model Using Fuzzy Logic Theory*, High Voltage Engineering (in Chinese), vol. 37, no. 5, pp. 1245–1252 (2011), DOI: 10.13336/j.1003-6520.hve.2011.05.026.

[14] Li Xianchu, Zhang Xi, Liu Jie *et al.*, *AMPSO-BP neural network prediction model for transmission line wire icing*, Power Construction (in Chinese), vol. 42, no. 9, pp. 140–146 (2021), DOI: 10.12204/j.issn.1000-7229.2021.09.015.

[15] Wu Lei, Xu Mengnan, Zhang Huapeng *et al.*, *Simulation analysis of impact vibration de-icing on electrified railway contact network*, Railway Journal (in Chinese), vol. 47, no. 1, pp. 47–53 (2025), DOI: 10.3969/j.issn.1001-8360.2025.01.006.

[16] Li Junbo, Bao Yun, Shi Weifeng *et al.*, *Railway contact network ice analysis and prevention measures*, China Railway (in Chinese), no. 1, pp. 134–139 (2025), DOI: 10.19549/j.issn.1001-683x.2024.04.09.001.

[17] Ling Fei, *Research on contact network ice cover prediction method based on RBF neural network*, China Equipment Engineering (in Chinese), no. 16, pp. 251–253 (2024), DOI: 10.3969/j.issn.1671-0711.2024.16.105.

[18] Wang Zhen, Lin Sheng, Feng Ding *et al.*, *Research on contact network reliability assessment method considering weather conditions*, Journal of Railway (in Chinese), vol. 40, no. 10, pp. 49–56 (2018), DOI: 10.3969/j.issn.1001-8360.2018.10.008.

[19] Fritjof Nilsson, Ali Moyassari, Ángela Bautista *et al.*, *Modelling anti-icing of railway overhead catenary wires by resistive heating*, International Journal of Heat and Mass Transfer, vol. 143, 118505, ISSN 0017-9310 (2019), DOI: 10.1016/j.ijheatmasstransfer.2019.118505.

[20] Skrzyniarz Marek, Kruczek Włodzimierz, Mike Kamil, Stypułkowski Piotr, *Development of a model of current distribution in the overhead contact lines for an innovative de-icing system*, Problemy Kolejnictwa (2022), DOI: 10.36137/1956E.

[21] Lotfi Arefeh, Muhammad S. Virk, *Railway operations in icing conditions: a review of issues and mitigation methods*, Public Transport, vol. 15, no. 3, pp. 747–765 (2023), DOI: 10.1007/s12469-023-00327-6.

[22] Zhou Chengning, *Research on Surrogate Model-based Structural Reliability Method under Stochastic and Cognitive Uncertainty*, University of Electronic Science and Technology of China (in Chinese) (2021), DOI: 10.27005/d.cnki.gdzku.2021.000197.

[23] Yu Zhenliang, Sun Zhili, Zhang Yibo *et al.*, *A structural reliability analysis method for adaptive PC-Kriging model*, Journal of Northeastern University (Natural Science) (in Chinese), vol. 41, no. 5, pp. 667–672 (2020), DOI: 10.12068/j.issn.1005-3026.2020.05.010.

[24] Gao Jin, Cui Haibing, Fan Tao *et al.*, *A structural reliability analysis method based on adaptive Kriging ensemble model*, China Mechanical Engineering (in Chinese), vol. 35, no. 1, pp. 83–92 (2024), DOI: 10.3969/j.issn.1004-132X.2024.01.008.

[25] Ouyang Linhan, Huang Lei, Han Mei, *An Active Learning Reliability Analysis Algorithm: Based on the Perspective of Kriging Prediction Variance*, Systems Engineering Theory and Practice (in Chinese), vol. 43, no. 7, pp. 2154–2165 (2023), DOI: 10.12011/SETP2022-2399.

[26] Guo Lei, *Research on catenary icing mechanism and online anti-icing method*, Southwest Jiaotong University (in Chinese) (2013), DOI: 10.7666/d.Y2334434.

[27] Liu Lin, *Discussion on catenary icing monitoring and de-icing scheme*, China Academy of Railway Sciences (in Chinese) (2022), DOI: 10.27369/d.cnki.gtdky.2022.000093.

[28] Bing Junweng, Wei Gao, Wei Couzheng *et al.*, *Newly designed identifying method for ice thickness on high-voltage transmission lines via machine vision*, High Voltage, vol. 6, no. 5, pp. 904–922 (2021), DOI: 10.1049/hve2.12086.

[29] Fu Songping, Huang Guosheng, Qiao Zhen *et al.*, *Research on icing prediction and treatment scheme of railway catenary*, Railway Construction Technology (in Chinese), vol. 11, pp. 31–34 (2023), DOI: 10.3969/j.issn.1009-4539.2023.11.009.

[30] Li Zheng, Wu Guangning, Huang Guizao *et al.*, *Study on icing prediction for high-speed railway catenary oriented to numerical model and deep learning*, IEEE Transactions on Transportation Electrification (in Chinese), vol. 11, no. 1, pp. 1189–1200 (2025), DOI: 10.1109/TTE.2024.3401209.

[31] Feng Kaining, Gao Fei, *Characteristics and Forecast Model of Traverse Ice Covering in Inner Mongolia*, Journal of Green Science and Technology (in Chinese), vol. 25, no. 8, pp. 68–72+76 (2023), DOI: 10.16663/j.cnki.lskj.2023.08.011.